# Prompt and delayed Coulomb explosion of doubly ionized hydrogen chloride molecules in intense femtosecond laser fields

Junyang Ma,[1] Hui Li,[1,*] Kang Lin,[1] Qiying Song,[1] Qinying Ji,[1] Wenbin Zhang,[1] Hanxiao Li,[1] Fenghao Sun,[1] Junjie Qiang,[1] Peifen Lu,[1] Xiaochun Gong,[1] Heping Zeng,[1] and Jian Wu[1,2]

[1]*State Key Laboratory of Precision Spectroscopy, East China Normal University, Shanghai 200062, China*

[2]*Collaborative Innovation Center of Extreme Optics, Shanxi University, Taiyuan, Shanxi 030006, China*

(Received 4 April 2018; published 11 June 2018)

We experimentally investigate the dissociative double ionization of hydrogen chloride (HCl) molecules in intense femtosecond laser pulses. In addition to the prompt dissociation channels which occur on femtosecond timescales, long-lived hydrogen chloride dications which Coulomb-explode in flight towards the detector are clearly identified in the photoion-photoion coincidence spectrum. Different pathways leading to these prompt and delayed dissociation channels involving various bound and repulsive states of the HCl dication are discussed based on the observed kinetic energy release and momentum distributions. Our results indicate that the specific features of the HCl dication potential energy curves are responsible for the generation of the delayed fragmentation channels, which are expected to be general processes for the hydrogen halides.

DOI: 10.1103/PhysRevA.97.063407

## I. INTRODUCTION

When exposed to a strong laser field, a molecule can be ionized through multiphoton [1–7], tunneling [8–14], or over-the-barrier ionization processes [15], resulting in a certain charge state that may be dissociative and lead to the fragmentation of the molecular ion into several pieces. Among the abundant laser-driven phenomena in molecules, the dissociative double ionization exhibits a lot of intriguing characteristics, one of which is the unexpected enhanced double ionization rate from nonsequential double ionization [16–18]. For double ionization, enormous efforts have been made to explore the correlated dynamics for both the momenta and the kinetic energies of the two freed electrons [19,20]. Meanwhile, a lot of insights were gained for the molecular dynamics in the present of well-controlled laser fields utilizing advanced coincidence detection techniques [21,22]. The population of specific electronic states, thus the reaction quantum path in molecular systems, can be effectively manipulated by controlling the laser fields [23]. The rich structure of molecules gives rise to even more degrees of freedom for the dynamical manipulation.

Hydrogen chloride (HCl) [24] and its isotope DCl [25,26] have drawn lots of attention in the realm of strong-field physics due to their large dipole moments, well-studied potential energy curves (PECs), and rich fragmentation dynamics [27–29]. The tunneling contribution of the highest occupied molecular orbital (HOMO) and of the next lower-lying highest-energy molecular orbital (HOMO-1) can be distinguished for HCl, due to their distinct profiles and large difference of the binding energies [24]. The doubly ionized HCl molecule, which can be regarded as a prototype of heteronuclear molecular dication, still holds surprising, unique properties. In most cases, the field-induced molecular fragmentation from a dissociative state occurs on femtosecond to picosecond timescales [30,31]. However, there exist some metastable states characterized by deep minima in the PECs of the $HCl^{2+}$. The lifetime increases for the lower vibrational states of these metastable states and can reach nanosecond or microsecond timescales [32]. By removing the electrons in low-lying molecular orbitals, excited electronic states can be populated that might lead to delayed fragmentation for HCl molecules.

In the present work, the dissociative double ionization of hydrogen chloride molecules in femtosecond laser fields is investigated utilizing coincidence momentum imaging techniques. The neutral molecules are doubly ionized in the strong laser field by removal of two electrons and then the molecular dications dissociate through various pathways. Besides the laser-induced molecular fragmentation from a dissociative state which occurs on femtosecond timescales, molecular dications with long lifetimes ranging from nanoseconds to microseconds are also detected in our experiments. For the long-lived dications, the three-dimensional (3D) momentum distributions are found to be isotropic regardless of the laser field polarization. The delayed fragmentations from hydrocarbon dications in femtosecond laser fields have been observed in previous studies [33,34]. Our results demonstrate that such phenomena do not exist only in organic compounds such as $C_2H_2$ and $C_2H_4$ but also in inorganic molecules.

## II. EXPERIMENTAL SETUPS

The measurements were performed in a standard cold target recoil ion momentum spectroscope (COLTRIMS) [35,36] which is schematically illustrated in Fig. 1(a). Femtosecond laser pulses (25 fs, 790 nm, 10 kHz) produced from a multipass amplifier Ti:sapphire laser system propagates along the $x$ direction and are focused onto a supersonic gas jet in the vacuum chamber by a concave reflection mirror ($f = 75$ mm). The molecular beam is produced by coexpanding a mixture of

*hli@lps.ecnu.edu.cn

 

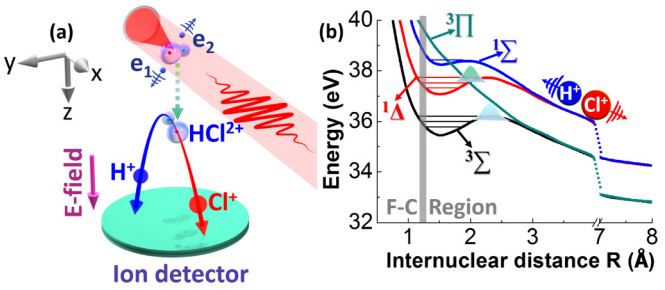


FIG. 1. (a) Schematic diagram of the experimental setup. The laser-induced dications are accelerated by a weak electric dc field and the fragments are detected in coincidence by the detector at the end of the spectrometer. (b) Relevant potential energy curves and vibrational levels of the $HCl^{2+}$ dication (adopted from [32]). The gray band indicates the Frank-Condon vertical transition region for the photoionization of neutral hydrogen chloride.

5% HCl and 95% He through a 30-$\mu$m nozzle with a driving pressure of 1.1 bar. The intensity of the linearly polarized laser field (polarized along the $y$ direction) is estimated to be around $3.4 \times 10^{14}\,\mathrm{W/cm^2}$. In order to trace the pathway of various dissociation channels, the polarization of the laser pulses is adjusted to be elliptical by using a half-wave plate and a quarter-wave plate. The peak intensity and ellipticity of the laser field are measured to be $I \sim 9.0 \times 10^{14}\,\mathrm{W/cm^2}$ and $\varepsilon \sim 0.72$, with major and minor polarization axes along the $y$ and the $z$ axis, respectively. Such an ellipticity is selected to optimize the data statistics and the momentum resolution in the measurement [36,37]. For the laser intensities used in this work, the Keldysh parameters are estimated to be smaller than 1 (the ionization potential of HCl is about 12.75 eV [24]); thus it lies in the tunneling ionization regime.

In our experiment, the dissociative double ionization of hydrogen chloride molecules is explored by detecting the ionic fragments in coincidence. The ions ejected from the multiply ionized molecules are accelerated and guided by a weak homogeneous static electric field (~14.2 V/cm) and are detected by a time- and position-sensitive microchannel plate detector at the end of the spectrometer. The 3D momenta of the detected ions are retrieved from the measured time of flights (TOFs) and positions of the impacts. Atomic units (a.u.) are used throughout this paper unless otherwise specified.

## III. RESULTS AND DISCUSSIONS

The photoion-photoion-coincidence (PIPICO) spectra of HCl for the dissociative double ionization channel is plotted in Fig. 2(a). The Coulomb-explosion channel $HCl \rightarrow H^+ + Cl^+ + 2e^-$ is denoted as HCl (1,1) in the following discussions. Two channels can be distinguished from the long parabolic PIPICO curve: the prompt fragmentation channel that dominates the yield of $H^+$ ions for the TOF smaller than about 1150 ns, and the long-tail distributions that extend beyond 1300 ns. These two channels overlap in the TOF region between 1150 and 1300 ns and can be clearly distinguished based on their inherent separation in the PIPICO which is shown in Fig. 2(a). Note that the long PIPICO curves are observed for both $H^{35}Cl$ and $H^{37}Cl$. Here we focus on the

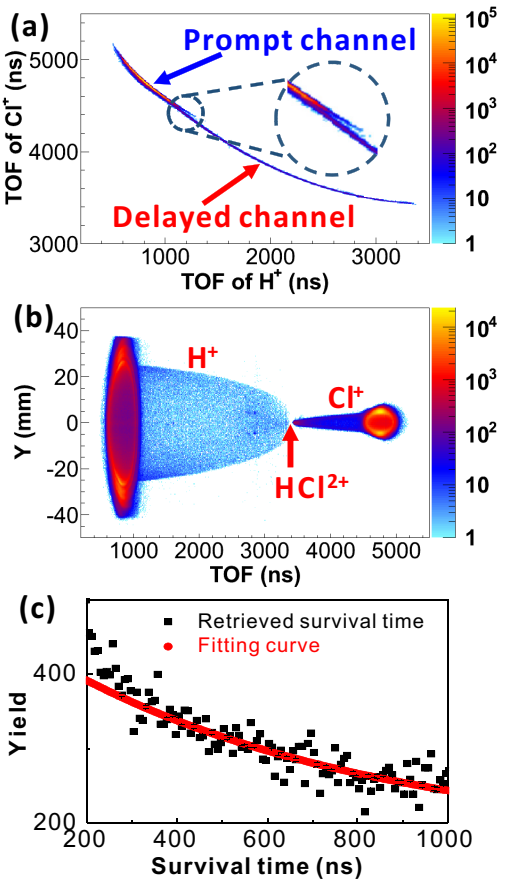


FIG. 2. (a) The PIPICO spectrum of the hydrogen chloride molecules for the dissociative double ionization channel, i.e., the HCl (1,1) channel, induced by linearly polarized femtosecond laser pulses at the laser intensity of $3.4 \times 10^{14}\,\mathrm{W/cm^2}$. (b) The ion yield as a function of the TOF and the $y$ position. The red arrow indicates the position of hydrogen chloride dications. (c) Retrieved survival time distributions of the hydrogen chloride dications fitted with an exponential function of $288.8\exp[-(1.43 \pm 0.067) \times 10^{-3}\,\mathrm{ns^{-1}} \times t]$.

$H^{35}Cl$ which exhibits larger natural abundance (around 75%). According to previous studies on the dissociative double ionization of hydrocarbon molecules in intense laser fields [33], the long PIPICO curve may indicate high kinetic energy release (KER) during Coulomb explosion. However, the TOF of either the $H^+$ or the $Cl^+$ corresponding to high KER only extends in one direction as shown in Fig. 2(b), which infers a different mechanism [38–40]. Moreover, when calculating the KER for the long PIPICO curve based on the assumption that the fragmentation is formed on femtosecond timescales, the resulting KER ranges extend from several eV to hundreds of eV as the TOF of $H^+$ increases, which is counterintuitive. On the other hand, a long PIPICO curve can likely be formed when there is a delay between the ionization and the Coulomb explosion; i.e., fragmentation occurs during the flight of the long-lived $HCl^{2+}$ to the detector. Based on this, we solved the Newton's equations of motion for the charged fragments in the weak dc field of the spectrometer to obtain the time interval between the double ionization and the fragmentation [33]. The

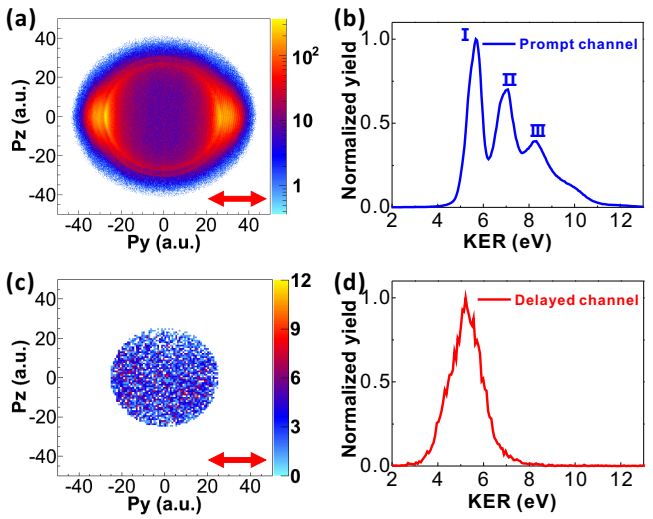


FIG. 3. (a) The momentum distributions of the ionic fragments in the $y$-$z$ plane and (b) the corresponding KER spectrum for the prompt Coulomb-explosion channel in linearly polarized femtosecond laser fields. The three distinct peaks centered around 5.7, 7.0, and 8.2 eV are marked as peaks I, II and III, respectively. (c,d) The same as (a,b) but for the delayed fragmentation channel. The red arrows in (a,c) indicate the polarization direction of the laser field.

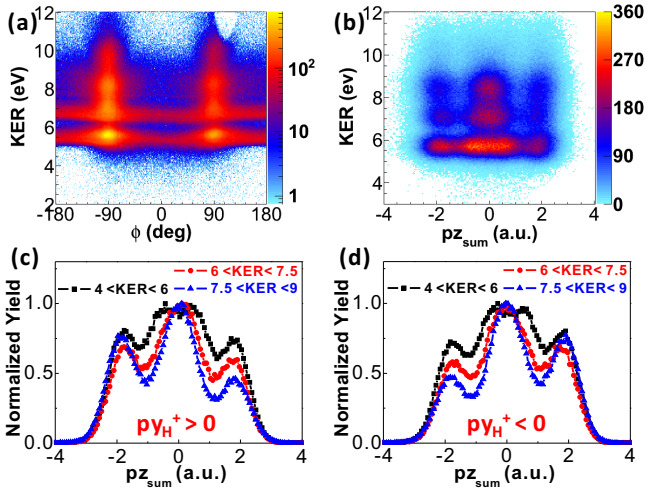


FIG. 4. (a) The KER-dependent angular distributions of the ionic fragments for the HCl(1,1) prompt channel in the polarization plane (the $y$-$z$ plane) in linearly polarized laser fields. (b) The KER-dependent ion sum-momentum distributions along the $z$ axis for the HCl(1,1) prompt channel with the molecular bond oriented within a cone of 45° about the $y$ axis in elliptically polarized laser fields. The projections over different KER ranges (as indicated in the figures) are shown for the $H^+$ emissions to the (c) the $+y$ direction and (d) the $-y$ direction, respectively.

initial momentum of the dication is assumed to be zero in the calculation. Before fragmentation, the dication flies towards the detector as a whole. When fragmentation takes place, the $HCl^{2+}$ dication breaks into $H^+$ and $Cl^+$ ions which fly towards the ion detector and hit at different times and positions. The two fragment ions fulfill momentum conservation to ensure coincidence selection in the off-line data analysis. In this case, the neutral HCl molecules are doubly ionized by the laser field, and the dications afterwards dissociate after a nanosecond to microsecond lifetime. Note that such a "delayed channel" is also obtained when using elliptically or circularly polarized femtosecond laser pulses, which will be discussed elsewhere.

The momentum distributions in the $y$-$z$ plane and the KER spectra are shown for the prompt and the delayed Coulomb-explosion channels in Fig. 3. Laser-induced molecular fragmentation from a dissociative state forms the prompt channel which occurs on femtosecond timescales. For this channel, distinct ring structures can be observed in the momentum maps in Fig. 3(a). These ring structures form the peaks in the KER spectrum centered around 5.7, 7.0, and 8.2 eV (marked as I, II, and III) shown in Fig. 3 (b). As shown in Fig. 4(a), we note that the yields corresponding to the KER peaks I and II in Fig. 3(b) exhibit broad angular distributions with more events being detected along the polarization direction, while the higher KER components beyond 8 eV show narrower angular distributions around the $y$ direction. Both the angular and the KER distributions agree fairly well with previous measurements performed in few-cycle near-infrared laser fields [25,26]. The angular distributions for peaks I–III can be attributed to orientation-dependent ionization of the HCl molecules. Here, we focus on the dissociative double ionization of HCl in strong laser fields where several excited states of $HCl^{2+}$ are involved. The relevant PECs of the $HCl^{2+}$ are plotted in Fig. 1(b) [32]. The three lowest electronic states ($^3\Sigma$, $^1\Delta$, $^1\Sigma$) of the hydrogen chloride dications are metastable states which are formed by removal of two electrons from the HOMO. The repulsive state $^3\Pi$ is, however, formed by removal of two individual electrons from the HOMO and the HOMO-1, respectively.

For the prompt HCl (1,1) channel, an elliptically polarized intense laser field is also utilized to distinguish the dissociation pathways by omitting the recollisional processes. The electrons being freed by the laser field pointing along the major axis will end up with a final momentum pointing along the minor axis due to the angular streaking of the rotating electric field. For the counterclockwise rotating electric fields, the electrons with final momentum along the $-z/+z$ axis are generated in the ionization events when the instantaneous laser field points to the $+y/-y$ directions [12,41–43]. The convoluted momentum distributions of the sequentially emitted electrons are mapped on the ion sum-momentum distributions of the correlated ions (i.e., $pz_{\rm sum} = pz_{\rm ion1} + pz_{\rm ion2}$) according to the law of momentum conservation of the breaking molecule. Figure 4(b) shows the KER-dependent ion sum-momentum distributions of the HCl (1,1) channel along the $z$ axis (the minor axis of the elliptically polarized laser field). To optimize the signal-to-noise ratio and to maintain enough data statistics, only fragment ions emitting within a cone of 45° with respect to the $y$ axis are considered here. Three distinct peaks around 0 and $\pm 1.8$ a.u. can be identified which indicate different emission properties of the sequentially released electrons in double ionization [41–43]. The distribution around $pz_{\rm sum} = 0$ a.u. results from the double ionization events when the two electrons are ejected to the opposite directions. The two side peaks centered at $pz_{\rm sum} = \pm 1.8$ a.u. are mainly contributed by events where both electrons escape to the same side of

the molecules. As shown in Figs. 4(c) and 4(d), the KER-integrated ion sum-momentum distributions show asymmetric distributions when we select the $H^+$ ions emissions to the $+y$ or to the $-y$ directions. These asymmetric distributions are mainly governed by the shape of the molecular orbital from which the electron is emitted [41,42]. The HOMO of HCl is a $\pi$ orbital which is homogeneously distributed around the H and the Cl nuclei while the HOMO-1 (a $\sigma$ orbital) exhibits asymmetric distributions [24]. In Figs. 4(c) and 4(d), comparing to that of the two lower KER regions (<7.5 eV), larger asymmetry is obtained for the high KER range (7.5–9 eV), which indicates a possible contribution from the HOMO-1 in the double ionization process. However, if the two electrons are both from the HOMO-1, higher excitation states [not shown in Fig. 1(b)] will be populated which will result in disagreement in the KER distributions to the present measurements. Thus for the dissociative double ionization channel of HCl which yields ions with KER >7.5 eV it results from one electron being removed from the HOMO and the other is removed from the HOMO-1.

The three peaks in the KER spectrum for the prompt channel shown in Fig. 3(b) are expected to occur via different pathways. As shown in Figs. 4(a), 4(c), and 4(d), for the KER range between 4 and 6 eV [corresponding to peak I in Fig. 3(b)], the broader angular distributions in the polarization plane (the $y$-$z$ plane) and the smaller asymmetry in the ion sum-momentum distributions can be produced by removing two electrons from the HOMO and the population of the launched nuclear wave packet (NWP) on the ground state $^3\Sigma$ of the molecular dication. By absorbing one extra photon, the NWP can be excited to the $^3\Pi$ repulsive state and dissociate into $H^+$ and $Cl^+$ ions. For peak II (corresponding to KER in the range of 6–7.5 eV), two electrons are removed from the HOMO and the NWP is excited to the $^1\Delta$ state; then the NWP can be further excited to the $^3\Pi$ state by field-induced coupling, where dissociation occurs. For peak III (with KER beyond 8.2 eV), the relatively narrow angular distributions in the polarization plane and the larger asymmetries obtained in the ion sum-momentum distributions indicate that the two individual electrons are removed from the HOMO and the HOMO-1, respectively, accompanied by the NWP being excited directly to the higher-energy regions on the repulsive $^3\Pi$ state.

We now discuss the formation of the delayed Coulomb explosion of the long-lived dication. The momentum distributions in the $y$-$z$ plane and the KER spectra of the fragment ions retrieved for the delayed fragmentation channel are shown in Figs. 3(c) and 3(d). Homogeneous angular distributions are obtained. The ion yield peaks at around 5.1 eV for the delayed channel. The relative channel strength of the delayed channel over the prompt one is around 1.6%. An intuitive explanation, as illustrated in Fig. 1(a), could be that the delayed fragmentation occurs during the flight of the long-lived $HCl^{2+}$ dication towards the detector. Due to the fact that the survival time of the $HCl^{2+}$ dication is much longer than its rotational period (∼1.6 ps), an isotropic angular distribution is expected. Such a mechanism is consistent with the distributions of the $H^+$ and the $Cl^+$ ions covering a wide shadow extending from the two fragments all the way towards the $HCl^{2+}$ spot on the TOF spectrum [shown in Fig. 2(b)]. The survival time of $HCl^{2+}$ is estimated by fitting the measured TOF signal to an exponential decay function $S(t) = S_0 e^{-\alpha t}$, and the results are shown in Fig. 2(c). A decay rate of $\alpha = (1.43 \pm 0.067) \times 10^{-3}\,\mathrm{ns}^{-1}$ corresponding to a lifetime of 698 ± 30 ns is obtained.

Here we provide an indication of the possible mechanisms behind the long lifetime of the $HCl^{2+}$ dications leading to the delayed fragmentation process. The bound states of $HCl^{2+}$ can be populated directly by removing two electrons from the HOMO in the presence of strong femtosecond laser fields. The launched NWP can populate a vibrational state near the dissociation threshold of the $^3\Sigma$ or the $^1\Delta$ state, which exhibits a small barrier at the internuclear distance around 2.4 Å, as illustrated in Fig. 1(b). The dications can then dissociate into an $H^+$ and a $Cl^+$ ion after a certain lifetime through tunneling. As theoretically predicted in Ref. [32], the lifetimes of several vibrational states of the $^3\Sigma$ and $^1\Delta$ states lie on the same timescale compared to our fitted results. The lifetime of the $^1\Sigma$ ground vibrational states is comparably small [32]; therefore the contribution from $^1\Sigma$ to the slow deprotonation process is insignificant in our experiment. Note that the main interaction components have been taken into account in the lifetime calculations, while some missing aspects can still affect the final results dramatically. For instance, calculations according to the potential energy curves have shown that the lifetimes of the vibrational states are very sensitive to the exact landscape of the potential energy curves [44]. Another possible mechanism could be that the NWP in the excited $^1\Delta$ state transits to the repulsive state $^3\Pi$ via spin-orbit coupling [33,44,45]. Such process can also yield fragment ions within the KER range that we detected here.

## IV. CONCLUSION

In conclusion, the dissociative double ionization of hydrogen chloride molecules in intense femtosecond laser pulses has been experimentally investigated. Both the prompt and the delayed dissociation channels were observed. Significant differences have been obtained between these two channels in both the momentum distributions and the KER spectra. Characteristic angular distributions originating from orientation-dependent ionization were detected for different KERs for the prompt channel, while the angular distributions were almost isotropic for the delayed fragmentation channel. Elliptically polarized laser pulses were utilized to distinguish various pathways for the prompt channel. The three KER ranges have been attributed to dissociative double ionization pathways involving laser-induced coupling from several excited bound states towards the $^3\Pi$ repulsive state following dissociation on ultrafast timescales. On the other hand, the observed long-lived (nanosecond to microsecond timescales) hydrogen chloride dications can be attributed to tunneling from the long-lived vibrational states near the dissociation threshold of the $^3\Sigma$ and the $^1\Delta$ bound states or spin-orbit coupling between the bound and the repulsive electronic states. Our method based on coincidence momentum detection can serve as a general tool to explore the various dissociation pathways in molecular dissociative double ionization, including the dissociation of long-lived molecular dications. Similar phenomena are expected to be observed in other hydrogen halides, such as HBr and HI.

**ACKNOWLEDGMENTS**

This work is supported by the National Key R&D Program of China (Grant No. 2018YFA0306303), the National Natural Science Fund of China (Grants No. 11704124, No. 11425416, No. 61690224, and No. 11761141004), the 111 project of China (Grant No. B12024), and the Shanghai Sailing Program (Grant No. 17YF1404000).

[1] Th. Weber, H. Giessen, M. Weckenbrock, G. Urbasch, A.Staudte, L. Spielberger, O. Jagutzki, V. Mergel, M. Vollmer, and R. Dörner, Nature (UK) **405**, 658 (2000).
[2] W. Becker, X. Liu, P. J. Ho, and J. H. Eberly, Rev. Mod. Phys. **84**, 1011 (2012).
[3] F. Krausz and M. Ivanov, Rev. Mod. Phys. **81**, 163 (2009).
[4] W. C. Wallace, M. G. Pullen, D. E. Laban, O. Ghafur, H. Xu, A. J. Palmer, G. F. Hanne, K. Bartschat, A. N. Grum-Grzhimailo, H. M. Quiney, I. V. Litvinyuk, R. T. Sang, and D. Kielpinski, New J. Phys. **15**, 033002 (2013).
[5] E. V. van der Zwan and M. Lein, Phys. Rev. Lett. **108**, 043004 (2012).
[6] P. Agostini, F. Fabre, G. Mainfray, G. Petite, and N. K. Rahman, Phys. Rev. Lett. **42**, 1127 (1979).
[7] D. Pengel, S. Kerbstadt, D. Johannmeyer, L. Englert, T. Bayer, and M. Wollenhaupt, Phys. Rev. Lett. **118**, 053003 (2017).
[8] J.-P. Wang and F. He, Phys. Rev. A **95**, 043420 (2017).
[9] K. Liu and I. Barth, Phys. Rev. Lett. **119**, 243204 (2017).
[10] Y. Liu, L. Fu, D. Ye, J. Liu, M. Li, C. Wu, Q. Gong, R. Moshammer, and J. Ullrich, Phys. Rev. Lett. **112**, 013003 (2014).
[11] T. Nubbemeyer, K. Gorling, A. Saenz, U. Eichmann, and W. Sandner, Phys. Rev. Lett. **101**, 233001 (2008).
[12] J. Wu, M. Meckel, L. Ph. H. Schmidt, M. Kunitski, S. Voss, H. Sann, H. Kim, T. Jahnke, A. Czasch, and R. Dörner, Nat. Commun. **3**, 1113 (2012).
[13] P. Tengdin, W. You, C. Chen, X. Shi, D. Zusin, Y. Zhang, C. Gentry, A. Blonsky, M. Keller, P. Oppeneer, H. Kapteyn, Z. Tao, and M. Murnane, Sci. Adv. **4**, 9744 (2018).
[14] X. M. Tong, Z. X. Zhao, and C. D. Lin, Phys. Rev. A **66**, 033402 (2002).
[15] J. S. Cohen, Phys. Rev. A **64**, 043412 (2001).
[16] B. Walker, B. Sheehy, L. F. DiMauro, P. Agostini, K. J. Schafer, and K. C. Kulander, Phys. Rev. Lett. **73**, 1227 (1994).
[17] N. Camus, B. Fischer, M. Kremer, V. Sharma, A. Rudenko, B. Bergues, M. Kubel, N. G. Johnson, M. F. Kling, T. Pfeifer, J. Ullrich, and R. Moshammer, Phys. Rev. Lett. **108**, 073003 (2012).
[18] X. Gong, Q. Song, Q. Ji, H. Pan, J. Ding, J. Wu, and H. Zeng, Phys. Rev. Lett. **112**, 243001 (2014).
[19] B. Bergues, M. Kübel, N. G. Johnson, B. Fischer, N. Camus, K. J. Betsch, O. Herrwerth, A. Senftleben, A. M. Sayler, T. Rathje, T. Pfeifer, I. Ben-Itzhak, R. R. Jones, G. G. Paulus, F. Krausz, R. Moshammer, J. Ullrich, and M. F. Kling, Nat. Commun. **3**, 813 (2012).
[20] X. Gong, Q. Song, Q. Ji, K. Lin, H. Pan, J. Ding, H. Zeng, and J. Wu, Phys. Rev. Lett. **114**, 163001 (2015).
[21] R. Dörner, V. Mergel, O. Jagutzki, L. Spielberger, J. Ullrich, R. Moshammer, and H. Schmidt-Böcking, Phys. Rep. **330**, 95 (2000).
[22] A. T. J. B. Eppink and D. H. Parker, Rev. Sci. Instrum. **68**, 3477 (1997).
[23] M. Kübel, A. S. Alnaser, B. Bergues, T. Pischke, J. Schmidt, Y. Deng, C. Jendrzejewski, J. Ullrich, G. G. Paulus, A. M. Azzeer, U. Kleineberg, R. Moshammer, and M. F. Kling, New J. Phys. **16**, 065017 (2014).
[24] H. Akagi, T. Otobe, A. Staudte, A. Shiner, F. Turner, R. Dörner, D. M. Villeneuve, and P. B. Corkum, Science **325**, 1364 (2009).
[25] H. Li, X. M. Tong, N. Schirmel, G. Urbasch, K. J. Betsch, S. Zherebtsov, F. Süßmann, A. Kessel, S. A. Trushin, G. G. Paulus, K.-M. Weitzel, and M. F. Kling, J. Phys. B **49**, 015601 (2016).
[26] I. Znakovskaya, P. von den Hoff, N. Schirmel, G. Urbasch, S. Zherebtsov, B. Bergues, R. de Vivie-Riedle, K.-M. Weitzel, and M. F. Kling, Phys. Chem. Chem. Phys. **13**, 8653 (2011).
[27] A. Fleischer, H. J. Worner, L. Arissian, L. R. Liu, M. Meckel, A. Rippert, R. Dörner, D. M. Villeneuve, P. B. Corkum, and A. Staudte, Phys. Rev. Lett. **107**, 113003 (2011).
[28] H. G. Breunig, A. Lauer, and K. M. Weitzel, J. Phys. Chem. A **110**, 6395 (2006).
[29] M. V. Korolkov and K. M. Weitzel, J. Chem. Theory Comput. **2**, 1492 (2006).
[30] A. S. Alnaser, I. Litvinyuk, T. Osipov, B. Ulrich, A. Landers, E. Wells, C. M. Maharjan, P. Ranitovic, I. Bochareva, D. Ray, and C. L. Cocke, J. Phys. B: At., Mol. Opt. Phys. **39**, S485 (2006).
[31] X. Zhou, P. Ranitovic, C. W. Hogle, J. H. D. Eland, H. C. Kapteyn, and M. M. Murnane, Nat. Phys. **8**, 232 (2012).
[32] M. M. Teixidor, F. Pirani, P. Candori, S. Falcinelli, and F. Vecchiocattivi, Chem. Phys. Lett. **379**, 139 (2003).
[33] S. Larimian, S. Erattupuzha, E. Lötstedt, T. Szidarovszky, R. Maurer, S. Roither, M. Schöffler, D. Kartashov, A. Baltuška, K. Yamanouchi, M. Kitzler, and X. Xie, Phys. Rev. A **93**, 053405 (2016).
[34] B. Jochim, R. Erdwien, Y. Malakar, T. Severt, B. Berry, P. Feizollah, J. Rajput, B. Kaderiya, W. L. Pearson, K. D. Carnes, A. Rudenko, and I. Ben-Itzhak, New J. Phys. **19**, 103006 (2017).
[35] X. Wang, H. Xu, A. Atia-Tul-Noor, B. T. Hu, D. Kielpinski, R. T. Sang, and I. V. Litvinyuk, Phys. Rev. Lett. **117**, 083003 (2016).
[36] J. Ullrich, R. Moshammer, A. Dorn, R. Dörner, L. Ph. H. Schmidt, and H. Schmidt-Böcking, Rep. Prog. Phys. **66**, 1463 (2003).
[37] J. Wu, X. Gong, M. Kunitski, F. K. Amankona-Diawuo, L. Ph. H. Schmidt, T. Jahnke, A. Czasch, T. Seideman, and R. Dörner, Phys. Rev. Lett. **111**, 083003 (2013).
[38] A. E. Slattery, T. A. Field, M. Ahmad, R. I. Hall, J. Lambourne, F. Penent, P. Lablanquie, and J. H. D. Eland, J. Chem. Phys. **122**, 084317 (2005).
[39] M. Alagia, C. Callegari, P. Candori, S. Falcinelli, F. Pirani, R. Richter, S. Stranges, and F. Vecchiocattivi, J. Chem. Phys. **136**, 204302 (2012).
[40] D. Holland, D. Shaw, I. Sumner, M. Bowler, R. Mackie, L. Shpinkova, L. Cooper, E. Rennie, J. Parker,

and C. Johnson, Int. J. Mass Spectrom. **220**, 31 (2002).

[41] J. Wu, L. Ph. H. Schmidt, M. Kunitski, M. Meckel, S. Voss, H. Sann, H. Kim, T. Jahnke, A. Czasch, and R. Dörner, Phys. Rev. Lett. **108**, 183001 (2012).

[42] Y. Sakemi, S. Minemoto, and H. Sakai, Phys. Rev. A **96**, 011401(R) (2017).

[43] F. Afaneh and H. Schmidt-Böcking, Int. J. Mod. Phys. B **31**, 1750215 (2017).

[44] M. Alagia, M. Boustimi, B. G. Brunetti, P. Candori, S. Falcinelli, R. Richter, S. Stranges, and F. Vecchiocattivi, J. Chem. Phys. **117**, 1098 (2002).

[45] S. Taylor, J. H. D. Eland, and M. Hochlaf, J. Chem. Phys. **124**, 204319 (2006).